Research Article Vol. 3, No. 4 / 15 Apr 2024 / Optics Continuum 552
OPTICS CONTINUUM

Influence of laser pulse shape and cleanliness on two-photon microscopy

SHAU POH CHONG[1,*] AND PETER TÖRÖK[1,2,3,4]

[1]Singapore Centre for Environmental Life Sciences Engineering (SCELSE), Nanyang Technological University, 60 Nanyang Drive, Singapore 637551, Singapore
[2]Lee Kong Chian School of Medicine, Nanyang Technological University, 59 Nanyang Drive, Singapore 639798, Singapore
[3]School of Physical and Mathematical Sciences, Nanyang Technological University, 50 Nanyang Drive, Singapore 639798, Singapore
[4]Institute for Digital Molecular Analytics and Science (IDMxS), 59 Nanyang Drive, Singapore 639798, Singapore
*josiah.chong@ntu.edu.sg

Abstract: Nonlinear microscopy, including two-photon microscopy, requires pulsed lasers as light source. Typically, when choosing the appropriate pulsed laser for two-photon microscopy, the pulse repetition rate, pulse width, total power output, and output beam diameter are among the critical parameters which are often emphasised. Here, we demonstrate that the pulse shape, often overlooked, can have significant impact on the two-photon microscopy excitation efficiency and the effective signal brightness. We provide metrics to ease practical selection of pulsed laser sources for two-photon microscopy.

© 2024 Optica Publishing Group under the terms of the Optica Open Access Publishing Agreement

1. Introduction

Two-photon fluorescence microscopes (2PM) employing near-infrared (NIR) lasers emitting femtosecond pulses have enabled effective imaging with sub-micron transverse resolution into highly-scattering biological samples such as rodents' brain and zebrafish with unprecedented penetration depths [1,2]. This is mainly due to weaker scattering of NIR light, as compared to visible, in biological tissues and the two-photon fluorescence excitation that reduces the out-of-focus fluorescence background. Since the last decade, fixed wavelength fiber based pulsed lasers are gaining popularity over solid state pulsed lasers, such as Ti: Sapphire lasers, mainly due to their competitiveness in terms of price, portability and low maintenance [3,4]. The efficiency of two-photon fluorescence excitation depends on the high spatio-temporal concentration of photons at the focal volume of the microscope objective lens, which necessitates the use of high numerical aperture (NA) lenses and femtosecond-pulsed lasers. Due to the fact that a laser source is typically the single most expensive part of a two-photon microscope, choosing the right femtosecond laser is the most important problem when designing a two-photon microscope [5].

When choosing the laser source, the pulse repetition rate, pulse width, beam diameter, its transverse intensity profile and power are among the critical parameters that must be considered [6,7]. For an average excitation power P, the number of fluorescent photons generated per fluorophore per laser pulse F at depth z is given by [8]:

$$F(z) = \frac{\eta\sigma}{\tau f^2}\left(\frac{\mathrm{NA}^2}{2\hbar c\lambda}\right)^2 P^2 \exp\left(\frac{-2z}{l_s}\right), \tag{1}$$

where η is the quantum efficiency of the two-photon generation process, σ is the two-photon absorption cross-section, τ is the laser pulse width (typically defined in full-wdith-half-maximum, FWHM), f is the repetition rate, l_s is the tissue scattering length, c is the speed of light, $\hbar$ is the reduced Plank constant, and λ is the centre wavelength. Note that even though the above

#515123 https://doi.org/10.1364/OPTCON.515123
Journal © 2024 Received 18 Dec 2023; revised 5 Mar 2024; accepted 6 Mar 2024; published 21 Mar 2024

OPTICS CONTINUUM

expression assumes a lens illuminated by a beam of uniform transverse intensity and the paraxial approximation, the application of high aperture focusing theory would not change the general dependency on the quantities of interest investigated in this work.

Equation (1) does not contain information regarding the temporal shape of the laser pulse apart from its pulse width. When a shape-related parameter is introduced [9] it enters into the equation as a constant multiplier because it is calculated as the temporal integral of the pulse intensity squared over a single pulse period (assuming mode-locked operation). A "two-photon advantage factor" was previously described by Denk *et al.* [10], ξ, which is given by

$$\xi = \frac{\langle P^2 \rangle}{\langle P \rangle^2} = (t_1 - t_2) \frac{\int_{t_1}^{t_2} P^2(t)\, dt}{\left[\int_{t_1}^{t_2} P(t)\, dt\right]^2}, \tag{2}$$

where $t_1 - t_2 = 1/f$ (i.e. pulse period T), emphasising the dependence of the two photon excitation efficiency upon not only the pulse duration but also the pulse shape [11]. Although McConnell [12] previously calculated the effect of different pulse shapes on the probability of two-photon absorption for specific laser parameters (i.e. $\tau = 200$ fs and $f = 80$ MHz), to the best of our knowledge, no scientific work has been published to investigate and demonstrate experimentally the effect of pulse shape (with similar or equal pulse widths) on two-photon excited fluorescence in terms of what happens to the energy within the pulse that does not go into two-photon excitation. While pulse shaping could be implemented to obtain the desired spectral or temporal pulse shape [13–15], it often requires complicated and expensive setup with low optical efficiency.

In the current work, we demonstrate that the pulse shape, or more precisely its deviation from the usual $\mathrm{sech}^2(t)$ time evolution, plays an important role in two-photon fluorescence imaging and the achievable signal-to-noise ratio (SNR) for a given average excitation power P, despite the same or similar τ.

2. Methods

2.1. Characterisation of the laser pulse

Using an autocorrelator (APE pulseCheck NX, Berlin, Germany), we measured the autocorrelation traces of two, fixed wavelength ($\lambda = 920$nm), fibre lasers (Spark Alcor 920, Serial number 2000104 – Laser 1, and Toptica FemtoFiber ultra 920, Serial number 01101 – Laser 2). Both of the lasers have pulse repetition rate of 80 MHz. The light emitted from the two lasers was directed to the autocorrelator by the same number and type of protected silver mirrors (see Supplement 1 Figure S5 for more information). Polarisation of the beams was adjusted so as to ensure maximum autocorrelation intensity. The pulse widths were optimised by the built-in dispersion pre-compensation module (GDD) in both lasers. The autocorrelator (using the built-in software) determined the pulse widths for Laser 1 and Laser 2 to be 108 and 95 fs, respectively. It is noted that the measured pulse widths match the specifications provided by the laser manufacturers, who on their websites claim 100 and <100 fs pulse duration, respectively [Laser 1 - https://spark-lasers.com/produit/alcor/; Laser 2 - https://www.toptica.com/products/psfs-fiber-lasers/femtofiber-ultra], whereas the calibration reports supplied with the lasers state 98.9 and 87.0 fs, respectively. Figure 1(a) shows the measured pulse shapes. It is interesting to point out that even though the autocorrelator measured the pulse widths to be different, which happened due to poor quality fit of the $\mathrm{sech}^2(t)$ function for Laser 1, when the traces are normalised and plotted on the same diagram Fig. 1(c) it is obvious that their respective pulse widths is almost identical. This fact will be important in later findings as, according to Eq. (1), in order to be able to directly compare two lasers and their use for two-photon imaging, their pulse width τ must be identical, or at least very similar.

OPTICS CONTINUUM

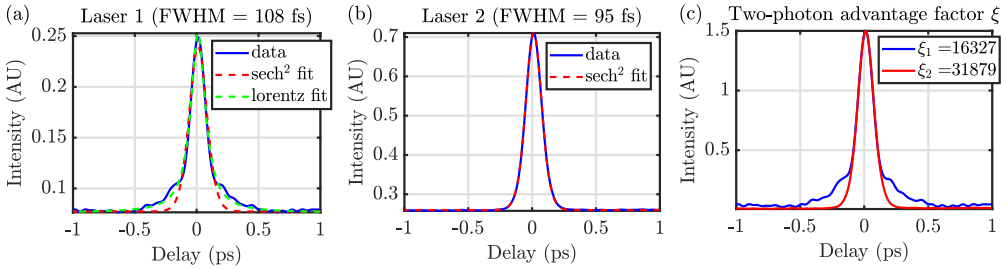

Fig. 1. (a) Autocorrelation traces of Laser 1 with their corresponding $\text{sech}^2(t)$ and Lorentzian fit. It is apparent that the pulse shape of Laser 1 more closely resembles Lorentzian shape. (b) Autocorrelation traces of Laser 2 with the corresponding $\text{sech}^2(t)$ fit. (c) Normalised pulse autocorrelation trace of Laser 1 and Laser 2. The calculated ξ is based on measured data in the [-1.5 ps , +1.5 ps] time interval only. ξ_1 and ξ_2 correspond to the Laser 1 (a) and Laser 2 (b) respectively. The pulse widths were optimised using the built-in dispersion compensation unit (GDD) for each laser.

Based on the Eq. (2), we calculated the two-photon advantage factor ξ with the caveat that the calculation was based on measured data in the $[t_L, t_U]$ time interval instead of the $t_1 - t_2 = 1/f$, (i.e. pulse period T is 12500 ps for the lasers; or $f = 80$ MHz) for the autocorrelation traces of Laser 1 and 2 in Fig. 1(a-b). We found $\xi = 16327$ and 31879 for Laser 1 and Laser 2, respectively meaning that the pulse of Laser 2 was approximately 1.95× more effective than Laser 1 in exciting two-photon absorption given the same FWHM pulse width and peak power.

We subsequently measured the spectra (Fig. 2(a)) of the lasers using an optical spectrum analyzer (AQ6370D, Yokogawa). The FWHM spectral bandwidth of Laser 1 and 2 were 17.36 nm and 12.17 nm, respectively. The transform-limited pulses were then calculated (through operation of Fourier Transform) based on the measured spectra (Fig. 2(b) for linear scale and Fig. 2(c) for log scale.), and their FWHM pulse width were also estimated. As the factory provided dispersion (pre or post)-compensation unit works for compensation of second order dispersion (GDD) only, any residual dispersion could be attributed to the presence of third order dispersion (TOD) which is known to cause pulse broadening [16]. This is evidently shown in Fig. 2(d,e) revealing that the laser pulses cannot be efficiently compressed to their theoretical limits due to the phase distortions.

The time–bandwidth product (TBP) of a light pulse is defined as the product of its temporal duration and spectral width (in frequency space) and is often used to determine how close a pulse is to the transform limit, i.e., how close the pulse duration is to the limit which is set by its spectral width. The minimum possible TBP is obtained for bandwidth-limited pulses. In other words, the TBP is an indicative whether a pulse is chirped, or phase distorted. For reference, the TBP is ≈ 0.315 for bandwidth-limited sech^2 shaped pulses and ≈ 0.44 for Gaussian pulses. Previously, it was also demonstrated that pulses compressed closer to transform-limited shape would optimize fluorescence yield [17].

Based on the measured spectral bandwidth, the pulse width, and setting the central wavelength as 920 nm, the TBP of Laser 1 and 2 are given in Table 1. As we assumed the pulse to be sech^2 shaped, the minimum TBP expected is ≈ 0.315. The closer the TBP is to 0.315, the more bandwidth-limited the pulse is, or in other words, the less phase distortion the pulse has. For the two lasers tested, Laser 2 exhibited the smaller TBP (Table 1), also evidenced by the lower side lobes in the autocorrelation traces (Fig. 3(b)).

A closer look at the unfiltered autocorrelation traces of the lasers (Fig. 3) also reveals significant side-lobes for Laser 1, indicating existence of residual dispersion which cannot be neglected. The

OPTICS CONTINUUM

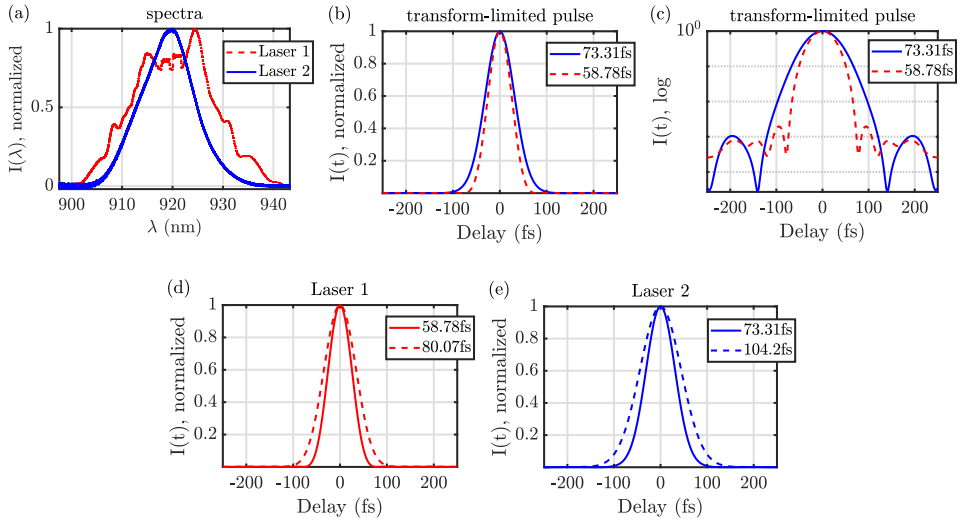

Fig. 2. (a) Spectra of the Laser 1 and Laser 2 and their transform-limited pulses (and FWHM pulse width) in linear (b) and log scale (c). Panel (a-c) share the same color scheme in which the red and blue corresponds to Laser 1 and 2 respectively. (d-e) The transform-limited pulse envelope (solid lines) and their self-convolution (dotted lines) which closely resemble the pulses measured using the autocorrelator. The pulse width values in the legends of panels (b-e) are FWHM pulse width).

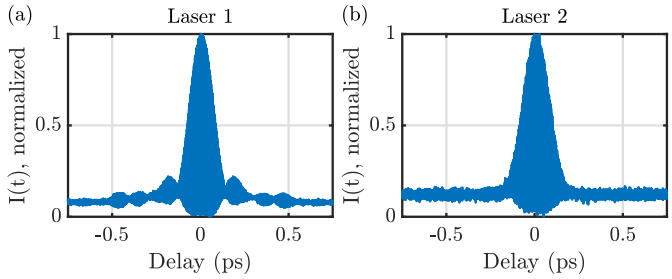

Fig. 3. Inteferometric autocorrelation traces of the (a) Laser 1 and (b) Laser 2. Evidently, there are significant sidelobes in the autocorrelation traces of Laser 1, indicating the existence of residual dispersion.

Table 1. Measured spectral bandwidth, FWHM pulse width and TBP of Laser 1 and 2 compared in the current study.

Laser	$\Delta\lambda$ (nm)	τ (fs)	TBP
Laser 1	17.36	108.0	0.664
Laser 2	12.17	95.4	0.411

OPTICS CONTINUUM

presence of this residual dispersion can prevent the pulses to be compressed close to their shortest possible width, that is theoretically only limited by their corresponding spectral bandwidths.

The purpose of the present work is to determine how the temporal evolution (shape) of the laser pulses affects two photon fluorescence excitation. Noting that the probability of two-photon fluorescence excitation is proportional to the square of the pulse intensity, the two-photon advantage factor ξ could describe the effect of the pulse shape in generating two-photon excitation. In comparison, for Laser 1 and Laser 2 the value of ξ, was found to be 16327 and 31879, respectively, meaning that, Laser 2 is almost 2× as effective as Laser 1 for two-photon excitation, at the same average power delivered to the sample. A direct consequence of this statement is that, if absorbed by the sample, almost 30 % of the light energy emitted by Laser 1 is dissipated by heating the sample when compared to Laser 2. This is problematic as excessive heating [18] can lead to undesirable photo-bleaching and photo-damage to a sample that is sensitive to heating such as zebrafish. This, in the opinion of the present authors, means that it is more advantageous to use Laser 2, or lasers that have similar ξ factor temporal pulse shapes, as opposed to using Laser 1, for two-photon imaging. In the second part of this paper, we test our hypothesis using a home-built two-photon microscope.

2.2. Two-photon microscope

In order to perform two-photon fluorescence microscope imaging we designed and built a bespoke two-photon microscope (Fig. 4, [19], please refer to Supplement 1 Fig S5 for the schematic of the two-photon microscope and setup for beam characterization.). Both Laser 1 and Laser 2, with integrated acousto-optic modulator (AOM) unit for power modulation, were used for illumination. The laser output beam was first expanded by a 2× reflective beam expander (#37-193, Canopus Reflective Beam Expanders, Edmund Optics, NJ, USA). The expanded beam (the measured beam diameters of Laser 1 and 2 were 3.75 mm and 4.01 mm respectively) was then directed into a scan engine module [20,21] constituting a pair of galvanometer scanners (Saturn 5B, ScannerMax) imaged by a pair of off-axis parabolic mirrors (#36-586, Edmund Optics, NJ, USA). Another version of scan engine module uses a 8-kHz resonant scanner mirror (CRS 8 kHz, Cambridge Technology) and a galvanometer scanner (6215H, Cambridge Technology). These modules are interchangeable in our system. The pixel dwell time for the resonant-galvo configuration is 80 ns, whereas it is 3.2 μs for the galvo-galvo configuration. The raster scanned laser beam is further expanded (5×) by the in-house designed scan and tube lens pair placed in a 4f configuration to overfill the back aperture of a water dipping objective lens (Zeiss Objective W "Plan-Apochromat" 20×/1.0, Jena, Germany). Before reaching the objective lens, the beam also passes through a long-pass dichroic mirror (BLP01-785R-35×50, Semrock).

The excited two-photon fluorescent light is collected by the same objective lens. The pupil of the objective lens is then imaged by two lenses (#38-327 and #45-094 Edmund Optics, NJ, USA) onto the light sensitive area of two photomultiplier tubes (PMT, H7422-40, Hamamatsu, Japan). This way there is no need to descan the fluorescent light as the image of the aperture stop of the objective lens on the PMT is always stationary with respect to the scanned illumination and also because the scanner mirrors are imaged onto each other and subsequently onto the aperture stop of the objective lens thus making the scanned beam stationary at that plane. In order to separate the two-photon emission from the excitation, the collected fluorescent light is reflected off by the long-pass dichroic mirror (BLP01-785R-35×50, Semrock) to separate the excitation and emission light paths. Then, the emission signal is further separated into a two-channel detection arrangement by a second dichroic mirror (FF562-Di03-38×45, Semrock) into green and red channels (emission filters FF01-520/70-18-D and FF01-593/46-18-D, Semrock) placed before the PMTs that are mounted on a heat sink so that the heat produced by their internal Peltier coolers can be dissipated. The heat sink is liquid cooled to a constant temperature of 20°C. The current signal generated by the PMTs is amplified by a home built transimpedance

OPTICS CONTINUUM

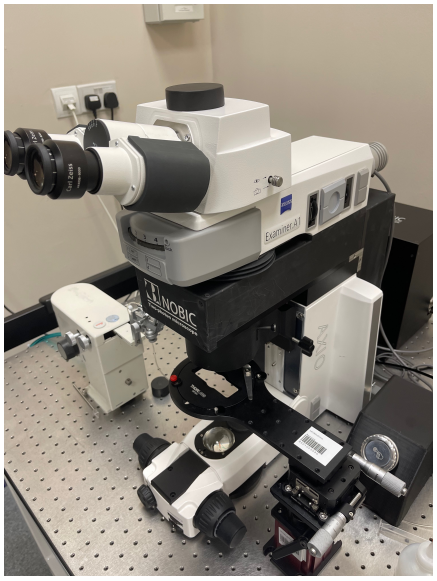

Fig. 4. A photo of the bespoke two-photon microscope. [19]

amplifier before being sent to a data acquisition device (vDAQ, ScanImage, Vidrio Technologies) for image digitisation/acquisition. The axial scanning is achieved by a piezo objective scanner (ND72Z2LAQ PIFOC Objective Scanning System 2000 μm), with a maximum total axial scanning range of 2000 μm. Scanning mirrors, piezo-objective scanner, AOMs, PMTs, and image acquisition were controlled with ScanImage software (Vidrio Technologies).

2.3. Imaging methods

Imaging was performed with fixed mouse brain slices and live zebrafish. Stack of images with 512×512 pixels were acquired. The light power after the objective lens was set to 2.9 mW and 7.3 mW, for galvo-galvo and resonant-galvo configuration respectively. The gain of the PMT was set to be the same throughout (control voltage around 0.6 V out of 0.9 V that corresponds to maximum gain, $\approx 10^5$ V/A) the whole imaging experiments. All the two-photon image pairs (Laser 1 vs Laser 2) are normalised to the maximum overall intensity in either image unless specified otherwise. Unless specified separately, all the images acquired with galvo-galvo configuration were presented with single exposure or without averaging; whereas all the images acquired with resonant-galvo configuration were presented with averaging of 10 frames. All procedures reported herein were carried out with the approval (A19062) of the Institutional Animal Care and Use Committee of the Nanyang Technological University, Singapore. All experiments were performed in accordance with the relevant guidelines and regulations for proper conduct of animal experiment and related activities.

2.3.1. Zebrafish

Tg(Xla.Tubb:jGCaMP7f [22,23]) 6 days post fertilization (dpf) larvae were anaesthetised with mivacurium and mounted dorsal side up in 2% low melting point agarose prepared in standard E3 solution (5 mM NaCl, 0.17 mM KCl, 0.33 mM $CaCl_2$, 0.33 mM $MgSO_4$). Fish were then mounted into a Nunc glass bottom dish (Thermofisher) filled with further E3 solution. Stimulus free spontaneous activity recordings were taken in the olfactory bulbs, and habenulae, using our custom-built two-photon microscope.

OPTICS CONTINUUM

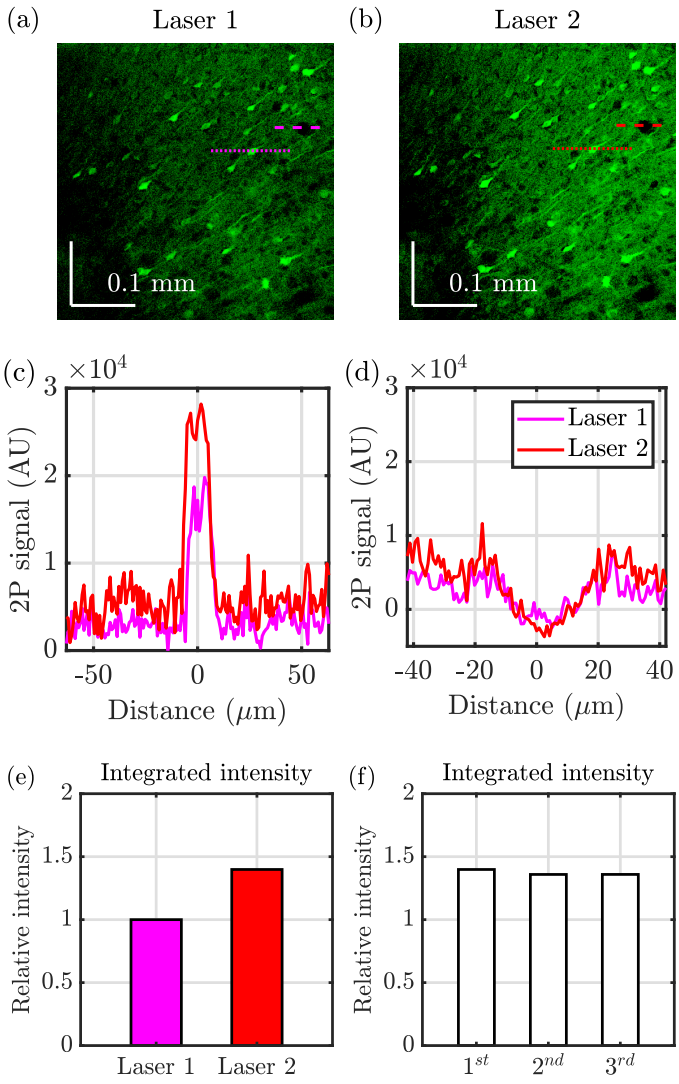

Fig. 5. Two-photon microscopy imaging of the gCAMP6s-labeled brain slice using (a) Laser 1 and (b) Laser 2. The galvo-galvo scanning configuration was employed for both of these images, with pixel dwell time 3.2 μs and average power under the objective lens 2.9 mW. Neuron soma and dendritic cells are readily resolvable. Scale bar is 100 μm. (c-d) Line profiles of the dotted and dashed lines in (a) and (b) showing that the signal level of across a soma (c) is approximately 40% higher for image captured by Laser 2, despite the same pixel dwell time and power. (d) Line profile (corresponds to dashed lines in (a) and (b)) showing a void in the images confirmed that both the images in (a-b) has approximate the same background levels. (c-d) share the same legend. (e) By calculating the integrated intensity of the image in (a) and (b) respectively, the overall increase in signal level is shown to be close to 40%. (f) We repeated the imaging of the same sample and observed consistent brightness improvement with Laser 2.

2.3.2. Mouse brain slice

Approximately 600–800 nL of AAV1-flex-GCaMP6f (100833-AAV1, Addgene) was injected into the brain of CaMKIIa-Cre mice through a borosilicate glass pipette using a microinjector

OPTICS CONTINUUM

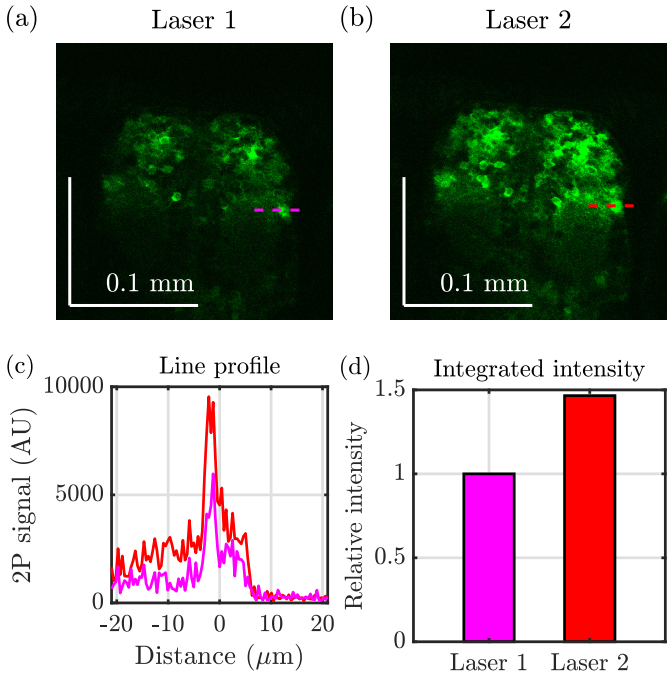

Fig. 6. Zebrafish imaging *in vivo* in the olfactory bulbs with neurons tagged with gCAMP7f acquired with (a) Laser 1 and (b) Laser 2, respectively. Scale bar is 100 μm. (c) Line profile of the dotted lines in (a) and (b) showing that the signal level across a soma is $\approx$ 47% higher for image captured by Laser 2, despite the same pixel dwell time of 3.2 μs and power 2.9 mW.(d) By calculating the integrated intensity of the image in (a) and (b), the overall increase in signal level is $\approx$ 47%.

(Nanoliter 2010, WPI). After finishing *in vivo* imaging experiments (typically 2-3 months after the injection), the mice were deeply anesthetized with isoflurane and immediately perfused with chilled 0.1 M PBS followed by 4% paraformaldehyde (wt/vol) in PBS. The brain was removed and post-fixed overnight at 4 °C. After fixation, the brain was placed in 30% sucrose (wt/vol) in PBS solution for 1–2 days at 4 C. After embedding and freezing, the brain was sectioned into 50μm coronal slices using a cryostat (Leica CM1950). The slides were mounted with Fluoroshield with DAPI (Sigma). Images were then taken using our custom-built two-photon microscope.

3. Imaging results

3.1. Galvo-galvo configuration

We performed imaging of mouse brain slices tagged with gCAMP6s, using the galvo-galvo scanning module, with average laser power under the objective lens set to 2.9mW for both Laser 1 and Laser 2 illumination as shown in Fig. 5(a) and (b), respectively. The signal level was optimised to the highest possible using the built-in dispersion pre-compensation module (GDD) of both Laser 1 and Laser 2 before image acquisition. In Fig. 5, we can clearly observe neuron soma and dendritic cells. From Fig. 5(a), the signal level of the soma is $\approx$ 40% higher when using Laser 2, while the background and noise levels (Fig. 5(b)) remain the same, representing a SNR improvement of $\approx$ 40%. The integrated intensity of the image in Fig. 5(a) and Fig. 5(b), reveals an overall increase in signal level of $\approx$ 40% as shown in Fig. 5(e). The signal improvement is repeatable as shown in Fig. 5(f).

OPTICS CONTINUUM

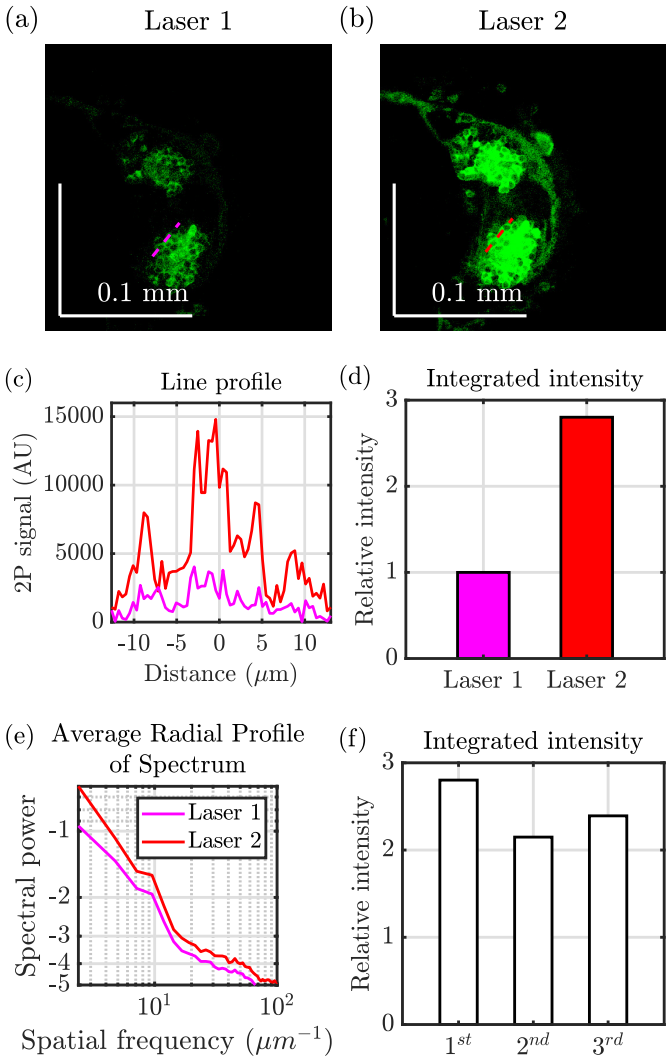

Fig. 7. Zebrafish habenulae imaging *in vivo* with neurons tagged with gCAMP7f acquired with (a) Laser 1 and (b) Laser 2. A resonant-galvo scanning configuration was employed when obtaining these images, with the power under the objective lens set to 7.3 mW for both lasers. The pixel dwell time is ≈ 80 ns. Five frames were averaged for both images. Scale bar is 100 μm. (c) Profile of the dotted lines in (a) and (b) showing that the signal level of across a soma is much higher for the image captured by Laser 2, despite the same pixel dwell time and excitation power. (d) By summing up the total intensity of the image in (a) and (b), the overall increase in signal level is found to be 2.8×. (e) Radially averaged profile of the spatial frequency spectrum of image (a) and (b). (f) We repeated the imaging of the same sample and observed consistent brightness improvement with Laser 2.

In the case of live zebrafish (Fig. 6(a) and (b)) we observed similar level of signal (Fig. 6(c)) improvement for the image acquired using Laser 2. The integrated intensity (Fig. 6(d)) of the images also reveals improvement in emitted fluorescent intensity.

OPTICS CONTINUUM

3.2. Resonant-galvo configuration

By switching the scanning module from galvo-galvo to resonant-galvo configuration, we increased the imaging speed by about ≈ 40× and imaged live zebrafish [24] with the power under the objective lens set to 7.3 mW, using both Laser 1 and Laser 2. Surprisingly, the improvement of the signal level is close to 2.8× from our images in Fig. 7. We attribute the increment of the signal level (compared to the galvo-galvo configuration) to the reduction in photobleaching (due to reduced pixel dwell time). We also observed a higher spectral power (Fig. 7(e)) of the image captured using Laser 2 as compared to Laser 1. We repeated imaging of the same zebrafish and the improvement of the signal level was reproducible (Fig. 7(f)).

4. Discussion

In the current study pulse shapes of a Spark Alcor 920 (Laser 1) laser and a Toptica FemtoFiber ultra 920 (Laser 2) were characterised and compared for their effectiveness to excite two-photon fluorescence. Our results show that the pulse width laser manufacturers often quote as the only shape related parameter is not sufficient to determine whether a laser is capable of efficiently exciting two-photon fluorescence. We have demonstrated experimentally, to the best of our knowledge for the first time, that the inherent temporal pulse shape of the laser (with similar or equal pulse widths) could result in vast differences in the achievable SNR.

We have observed as much as 2.8× increase in integrated intensity when using a higher ξ factor laser, in comparison to a lower ξ factor one, while the background intensity remained the same. It is noted that when we increased power of Laser 1 to 12 mW in order to boost the two-photon signal to the same level as that was at 7.3 mW illumination by Laser 2, the increased average power from Laser 1 resulted in the almost immediate destruction of the zebrafish which was believed to be due to heating of the sample [24,25].

It is worth mentioning that despite the shorter pixel dwell time for resonant-galvo scanning (80 ns) as compared to galvo-galvo scanning (3.2 μs), the power level needed for the resonant-galvo scanning configuration to produce two-photon microscope image of acceptable SNR does not require a power increase of 40× that would be expected from the dwell time difference [26]. This is due to the fast (resonant) scanning which reduces photobleaching [27] of the fluorophores during imaging [28–30]. As previously reported [30], for some fluorophores including green fluorescent protein, a 5–25-fold increase in total fluorescence yield could be observed when the dark or triplet state relaxation in the illumination process is avoided. Specifically, the triplet state relaxation with decay time in the μs range could prevent subsequent fluorescence signal generation when employing a relatively slow galvo-galvo scanning configuration despite having a much longer pixel dwell time. Hence, for our case when employing the resonant-galvo scanning configuration, the 2.5× higher power we used could effectively generate sufficient two-photon signal through reduction in photobleaching via lower laser dosage despite a pixel dwell time being 40× shorter.

It is interesting to observe that the improvement of the signal level for the pulse with $\mathrm{sech}^2(t)$ shape is greatly enhanced for fast resonant scanning. This implies that the pulse with $\mathrm{sech}^2(t)$ shape could better protect the sample from experiencing photobleaching than pulse in Lorentzian shape. Further work is needed to investigate the exact mechanism behind this observation.

The temporal pulse shape of a fiber laser is directly related to the mechanism of the lasing [31,32]. Specifically for Laser 2, the 920 nm pulse was generated by frequency doubling a 1840 nm pulse resulting in pulses with $\mathrm{sech}^2(t)$ shape [32]. It is possible to reshape the temporal shape of the pulse to remove the pedestals (or wings) through cubic phase correction [33] but expensive and sophisticated liquid crystal modulator is required. When comparing directly laser pulses of different pulse shapes, with the same FWHM pulse widths and peak power, as shown in Fig. 8(a), the amount of energy in the sidelobes could be quite different. Assuming the same 100 fs FWHM

OPTICS CONTINUUM

pulsewidth, their corresponding two-photon advantage factor ξ could vary by up to 2× depending on their intrinsic pulse shape as shown in Table 2.

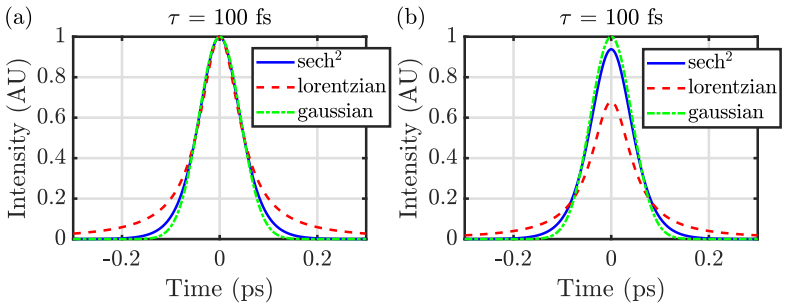

Fig. 8. (a) Comparison of $\text{sech}^2(t)$, Lorentzian and Gaussian laser pulses, all with the same 100 fs FWHM pulse width and unity peak power. (b) Comparison of $\text{sech}^2(t)$, Lorentzian and Gaussian laser pulses with their peak power scaled accordingly for the same pulse energies.

Table 2. Comparison of the two-photon advantage factor ξ_{norm} and peak powers $P_{\text{PEAK,norm}}$, both normalized to Gaussian pulse shape, for different pulse shapes and identical pulse energies.

Pulse shape	ξ_{norm}	$P_{\text{PEAK,norm}}$
Gaussian	1.0000	1.0000
sech^2	0.8845	0.9381
Lorentzian	0.4812	0.6785

Importantly, given the same pulse energies, a Lorentzian pulse will have only about 2/3 peak power when compared to sech^2 and Gaussian pulses (Fig. 8(b) and Table 2). As the two photon excitation efficiency scale quadratically with the pulse peak power, this will further limit the efficiency of Lorentzian pulse in two-photon microscopy.

5. Conclusion

We compared two fixed-wavelength fiber-based femtosecond pulsed lasers to investigate the influence of the pulse shape on the signal of the two-photon microscopy. We employed a custom-build modular two-photon microscope which allowed us to switch between galvo-galvo and resonant-galvo scanning configuration [26]. We showed that a $\text{sech}^2(t)$ shaped pulse is more efficient in generating two-photon signal than a Lorentzian pulse, for the same average power and pulse width. The improvement in SNR could be up to 2.8× for the case of fast resonant-galvo scanning configuration when imaging live zebrafish, due to lower photobleaching rate as well as higher excitation efficiency.

Funding. Nanyang Technological University; Lee Kong Chian School of Medicine, Nanyang Technological University.

Acknowledgments. We thank Toptica Photonics AG for loaning us the Toptica FemtoFiber ultra 920 laser employed in the current study and Dr. Manfred Karlowatz and Thomas Klos from Toptica Photonics AG for their insightful discussion on the technology behind the fiber laser systems relevant to the current study. We also thank Spark Lasers for loaning us the newer model of ALCOR 920-2-XSight with HPC technology (High Pulse Contrast) employed in the current study (i.e. Laser 3 in Supplement 1 information). We are very grateful for the long term collaboration with Carl Zeiss AG and are particularly thankful to Ralf Wolleschensky. Dr Michael Gölles of Carl Zeiss AG, Corporate

OPTICS CONTINUUM

Research & Technology provided much valued support with some aspects of optical design. We are grateful to Assistant Professor Tsukasa Kamigaki (NTU LKCM) for the provision of the mouse brain samples, A/Prof Suresh Jesuthasan and Mr Elliot Birkett (NTU LKCM) for the provision of the zebrafish sample. Mr Mohamed Aalim Khan, Mr Nicholas Mok and Mr Sayyed Omar Kamal Bin Syed Zin Al-Jufry have contributed to the design, construction and build of the two-photon microscope. **Author contributions statement**: S.P.C and P.T. conceived the experiment(s), S.P.C. conducted the experiment(s), S.P.C and P.T. analysed the results. Both authors reviewed the manuscript.

Disclosures. The study was carried out in compliance with the ARRIVE guidelines [34]. The authors declare that there are no conflicts of interest related to this article.

Data availability. All data that support the findings of this study are available from the corresponding author upon reasonable request.

Supplemental document. See Supplement 1 for supporting content.

References

1. F. Helmchen and W. Denk, "Deep tissue two-photon microscopy," Nat. Methods **2**(12), 932–940 (2005).
2. J. Lecoq, N. Orlova, and B. F. Grewe, "Wide. Fast. Deep: Recent Advances in Multiphoton Microscopy of *In Vivo* Neuronal Activity," J. Neurosci. **39**(46), 9042–9052 (2019).
3. C. Xu and F. W. Wise, "Recent advances in fibre lasers for nonlinear microscopy," Nat. Photonics **7**(11), 875–882 (2013).
4. T. Srinivasan and M. Yildirim, "Advances in Ultrafast Fiber Lasers for Multiphoton Microscopy in Neuroscience," Photonics **10**(12), 1307 (2023).
5. A. Andreev, "Two-photon microscopy and the $100,000 question: tunable or fixed-wavelength femtosecond laser?" https://www.laserfocusworld.com/lasers-sources/article/14185273/twophoton-microscopy-and-the-100000-question-tunable-or-fixedwavelength-femtosecond-laser (2020). Accessed: 2022-7-5.
6. C. Lefort, "A review of biomedical multiphoton microscopy and its laser sources," J. Phys. D: Appl. Phys. **50**(42), 423001 (2017).
7. S. Saidi and M. Shtrahman, "Evaluation of compact pulsed lasers for two-photon microscopy using a simple method for measuring two-photon excitation efficiency," Neurophotonics **10**(04), 044303 (2023).
8. J. P. Zinter and M. J. Levene, "Maximizing fluorescence collection efficiency in multiphoton microscopy," Opt. Express **19**(16), 15348–15362 (2011).
9. C. Xu and W. W. Webb, "Measurement of two-photon excitation cross sections of molecular fluorophores with data from 690 to 1050 nm," J. Opt. Soc. Am. B **13**(3), 481–491 (1996).
10. W. Denk, D. W. Piston, and W. W. Webb, "Two-Photon Molecular Excitation in Laser-Scanning Microscopy," Handbook of Biological Confocal Microscopy pp. 445–458 (1995).
11. J. J. Field, R. Carriles, K. E. Sheetz, *et al.*, "Optimizing the fluorescent yield in two-photon laser scanning microscopy with dispersion compensation," Opt. Express **18**(13), 13661 (2010).
12. G. McConnell, "Pulse shapes for optimized two-photon laser scanning microscopy," J. Phys. D: Appl. Phys. **41**(20), 205502 (2008).
13. A. Assion, T. Baumert, M. Bergt, *et al.*, "Control of chemical reactions by feedback-optimized phase-shaped femtosecond laser pulses," Science **282**(5390), 919–922 (1998).
14. A. Weiner, "Femtosecond optical pulse shaping and processing," Prog. Quantum Electron. **19**(3), 161–237 (1995).
15. A. M. Weiner, "Femtosecond pulse shaping using spatial light modulators," Rev. Sci. Instrum. **71**(5), 1929–1960 (2000).
16. D. M. Farinella, A. Roy, C. J. Liu, *et al.*, "Improving laser standards for three-photon microscopy," Neurophotonics **8**(01), 015009 (2021).
17. A. Fernández, L. Grüner-Nielsen, M. Andreana, *et al.*, "Optimizing pulse compressibility in completely all-fibered Ytterbium chirped pulse amplifiers for in vivo two photon laser scanning microscopy," Biomed. Opt. Express **8**(8), 3526 (2017).
18. K. Podgorski and G. Ranganathan, "Brain heating induced by near-infrared lasers during multiphoton microscopy," J. Neurophysiol. **116**(3), 1012–1023 (2016).
19. NOBIC, NOBIC (2024).http://www.nobic.sg
20. G. Sharafutdinova, J. Holdsworth, and D. van Helden, "Improved field scanner incorporating parabolic optics Part 1: Simulation," Appl. Opt. **48**(22), 4389–4396 (2009).
21. G. Sharafutdinova, J. Holdsworth, and D. van Helden, "Improved field scanner incorporating parabolic optics Part 2: experimental verification and potential for volume scanning," Appl. Opt. **49**(29), 5517–5527 (2010).
22. B. Podor, Y.-L. Hu, M. Ohkura, *et al.*, "Comparison of genetically encoded calcium indicators for monitoring action potentials in mammalian brain by two-photon excitation fluorescence microscopy," Neurophotonics **2**(2), 021014 (2015).
23. H. Dana, Y. Sun, B. Mohar, *et al.*, "High-performance calcium sensors for imaging activity in neuronal populations and microcompartments," Nat. Methods **16**(7), 649–657 (2019).
24. M. Bruzzone, E. Chiarello, M. Albanesi, *et al.*, "Whole brain functional recordings at cellular resolution in zebrafish larvae with 3D scanning multiphoton microscopy," Sci. Rep. **11**(1), 11048 (2021).

OPTICS CONTINUUM

25. M. J. Aragon, A. T. Mok, J. Shea, *et al.*, "Multiphoton imaging of neural structure and activity in drosophila through the intact cuticle," eLife **11**, e69094 (2022).
26. A. Zhou, S. A. Engelmann, S. A. Mihelic, *et al.*, "Evaluation of resonant scanning as a high-speed imaging technique for two-photon imaging of cortical vasculature," Biomed. Opt. Express **13**(3), 1374 (2022).
27. Y. Wu, X. Wu, R. Lu, *et al.*, "Resonant scanning with large field of view reduces photobleaching and enhances fluorescence yield in STED microscopy," Sci. Rep. **5**(1), 14766 (2015).
28. R. T. Borlinghaus, "MRT letter: high speed scanning has the potential to increase fluorescence yield and to reduce photobleaching," Microsc. Res. Tech. **69**(9), 689–692 (2006).
29. R. T. Borlinghaus, "Brighter fluorescence by resonant scanning," (2011).
30. G. Donnert, C. Eggeling, and S. W. Hell, "Major signal increase in fluorescence microscopy through dark-state relaxation," Nat. Methods **4**(1), 81–86 (2007).
31. P. Wang, X. Xu, Z. Guo, *et al.*, "926 nm Yb-doped fiber femtosecond laser system for two-photon microscopy," Appl. Phys. Express **12**(3), 032008 (2019).
32. C.-H. Hage, J.-T. Gomes, S. M. Bardet, *et al.*, "Two-photon microscopy with a frequency-doubled fully fusion-spliced fiber laser at 1840 nm," Opt. Lett. **43**(20), 5098–5101 (2018).
33. C.-C. Chang, H. P. Sardesai, and A. M. Weiner, "Dispersion-free fiber transmission for femtosecond pulses by use of a dispersion-compensating fiber and a programmable pulse shaper," Opt. Lett. **23**(4), 283 (1998).
34. ARRIVE *Animal Research: Reporting of In Vivo Experiments*, (2024). https://arriveguidelines.org

3.0.226.147 {ts '2024-07-24 02:38:45'}